

Using Sensor Signals to Analyze Fires

William D. Davis, Thomas Cleary, Michelle Donnelly and Samuel Hellerman
National Institute of Standards and Technology, Gaithersburg, MD. U.S.A.

Introduction

Building fire sensors are capable of supplying substantially more information to the fire service than just the simple detection of a possible fire. Nelson, in 1984, recognized the importance of tying all the building sensors to a smart fire panel.¹ In order to accomplish a smart fire panel configuration such as envisioned by Nelson, algorithms must be developed that convert the analog/digital signals received from sensors to the heat release rate (HRR) of the fire. Once the HRR of the fire is known, a multiroom zone fire model can be used to determine smoke layers and temperatures in the other rooms of the building. This information can then be sent to the fire service providing it with an approximate overview of the fire scenario in the building.

This paper will describe a ceiling jet algorithm that is being developed to predict the heat release rate (HRR) of a fire using signals from smoke and gas sensors. The prediction of this algorithm will be compared with experiments. In addition, an example of the predictions from a sensor-driven fire model, SDFM, using signals from heat sensors, will be compared with measurements from a full-scale, two-story, flashover townhouse fire.

Ceiling Jet Algorithm

The algorithm described below is an extension of a previously developed unconfined algorithm² that includes the impact of a developing smoke layer on the concentration of smoke in the ceiling jet. The following assumptions are made in order to simplify the equations. The fire is represented by a point source and assumed axisymmetric. The zone model approximation of homogeneous temperature and particle densities in each layer is assumed. The velocity, temperature, and smoke profiles in the plume are represented by Gaussian shapes in the radial direction. All air entrained into the plume below the smoke layer interface is considered to be smoke free. The deposition of smoke on surfaces is ignored.

The mass flux of smoke in a radially symmetric plume can be written as

$$\dot{m}_s(z) = \int_0^{\infty} C_{sp}(r,z)u_z(r,z)2\pi r dr$$

1

where $C_{sp}(r,z)$ is the mass concentration of smoke particles in the plume, $u_z(r,z)$ is the plume velocity, r is the radial distance from the plume centerline, and z is the height

above the fire source. The assumed Gaussian profiles for the smoke mass concentration in the plume and the plume velocity are,

$$C_{sp}(r, z) = C_{sp0}(z)e^{-(r^2/\lambda^2\sigma^2)} \quad 2$$

$$u_z(r, z) = u_{zm}(z)e^{(-r^2/\sigma^2)} \quad 3$$

where C_{sp0} is the smoke mass concentration for the plume centerline, u_{zm} is the plume centerline velocity, $\lambda\sigma$ is the $1/e$ width of the plume smoke profile and σ is the $1/e$ width of the velocity profile. It has been assumed that the smoke profile in the plume is equivalent to the temperature profile in the plume. Integrating equation 1 and solving for the maximum smoke mass concentration at the plume centerline gives

$$C_{sp0}(z) = \frac{\dot{m}_s(z)\left(\frac{\lambda^2 + 1}{\lambda^2}\right)}{u_{zm}(z)\pi\sigma^2} \quad 4$$

Using the plume correlations developed by Heskestad³ for $T(z)$, σ , u_{zm} and the location of the virtual point source, z_0 , the plume centerline smoke concentration is given by

$$C_{sp0}(\dot{Q}^*) = \frac{D\dot{Q}^{*2/3}}{(1 + K\dot{Q}^{*2/3})} \quad 5$$

$$\dot{Q}^* = \frac{\dot{Q}}{\rho_\infty c_p T_\infty g^2 Z^{5/2}} \quad 6$$

$$D = \frac{Y_s \left(\frac{\lambda^2 + 1}{\lambda^2} \right) \rho_\infty c_p T_\infty}{3.4 h_c \pi (1 - \chi_r)^{1/3} (1.201)^2 C_1^2} \quad 7$$

with $K=9.1(1-\chi_r)^{2/3}$, χ_r is the radiation fraction, Y_s is the smoke mass fraction, ρ_∞ and T_∞ are the ambient density and temperature, c_p is the heat capacity of air, g is the acceleration of gravity, h_c is the heat of combustion, $C_1=0.12^3$, and $Z=z-z_0$.

When a smoke layer is present, the plume centerline smoke concentration must be corrected for the entrained smoke as the smoke plume passes through the smoke layer. This can be approximated by replacing the fire with a substitute source and requiring that the plume produced by the substitute source be entirely in the smoke layer. The location and strength of the substitute source may be determined by requiring that the smoke mass flux at the layer interface be conserved and that the plume centerline smoke concentration be continuous across the layer interface. The requirement that the plume centerline smoke concentration be continuous across the layer interface is expressed by

$$C_{sp01} = C_{sp02} + C_L \quad 8$$

where C_L is the smoke concentration in the layer and the subscripts 1 and 2 refer to the plume centerline smoke concentration at the layer interface in the lower layer and the plume centerline smoke concentration from the substitute source in the smoke layer at the equivalent layer interface height. The subscript "1" is used for variables in the two-layer environment while subscript "2" is used for variables in the equivalent smoke layer environment. Using equation 5, the substitute source \dot{Q}_2^* is

$$\dot{Q}_2^* = \left[\frac{D\dot{Q}_1^{*2/3} - C_L(1 + k\dot{Q}_1^{*2/3})}{D + C_L K(1 + K\dot{Q}_1^{*2/3})} \right]^{3/2} \quad 9$$

The conservation of smoke mass flux at the boundary may be expressed by

$$\int_0^\infty C_{p1}(r, z) u_1(r, z) 2\pi r dr = \int_0^\infty (C_{p2}(r, z) + C_L) u_2 2\pi r dr \quad 10$$

Substituting equations 2, 3 and 5 into 10 and integrating yields the location of the substitute source with respect to the layer interface.

$$Z_2 = Z_1 \left[\frac{\dot{Q}_1^*}{\left(\dot{Q}_2^* + \frac{(\lambda^2 + 1) C_L}{D} (1 + K \dot{Q}_2^{*2/3}) \dot{Q}_2^{*1/3} \right)} \right]^{2/5} \quad 11$$

The requirement that the distance to the ceiling from the interface be identical for both calculations is satisfied by

$$H_2 - Z_2 = H_1 - Z_1 \quad 12$$

The plume centerline smoke concentration at the ceiling can then be calculated using the substitute source by

$$C_{sp0} = \frac{D \dot{Q}_2^{*2/3} \left(\frac{Z_2}{H_2} \right)^{5/3}}{\left(1 + K \dot{Q}_2^{*2/3} \left(\frac{Z_2}{H_2} \right)^{5/3} \right)} + C_L \quad 13$$

The next step is to obtain the smoke concentration in the ceiling jet using the calculated smoke concentration in the plume. Following Alpert's derivation⁴ and equating the mass flux in the plume to mass flux at the start of the ceiling jet, Yamauchi⁵ developed an equation which related the maximum smoke concentration in the plume at the ceiling, C_{sp0} to the average smoke concentration at the start of the ceiling jet, $C_{s,ave}$ in terms of the Gaussian width ratio λ for the velocity and temperature profiles in the plume. Assuming that the smoke concentration in the unconfined ceiling jet can be represented by a half Gaussian profile, the maximum smoke concentration in the ceiling jet in the presence of an upper layer, C_{s0} , is given by

$$C_{s0}(r = 0.18H) = \sqrt{2} \frac{\lambda^2}{1 + \lambda^2} (C_{sp0}(H) - C_L) + C_L \quad 14$$

where $\lambda^2 = 1.157^5$, r is the radial distance from the plume centerline and H is the distance from the surface of the fire to the ceiling. The smoke concentration in the ceiling jet may

be calculated from the smoke mass flux equation by integrating over the vertical dimension, y .

$$\frac{1}{r} \frac{d}{dr} \int_0^{\infty} [(C_s(r, y) - C_L) v(r, y) r dy] = 0 \quad 15$$

It has been assumed that there is no entrainment of smoke into the ceiling jet. The resulting spatial averages yield the average smoke concentration in the ceiling jet as a function of r as

$$C_s(r) = (C_s(r_e) - C_L) \frac{r_e v_e h_e}{r v h} + C_L \quad 16$$

where the subscript e represents the location where the ceiling jet forms ($r_e = 0.18H$), h is the average thickness of the ceiling jet, v is the average ceiling jet velocity and r is the radial distance from plume center. Using Alpert's correlation for the maximum ceiling jet velocity⁶ and fitting Alpert's calculation for ceiling jet thickness⁴ to a power law ($h/H \propto (r/H)^{0.4}$, $0.18H < r < 2.0H$), the maximum smoke concentration in the ceiling jet is given by

$$C_{s0}(r) = (C_{s0}(r_e) - C_L) \left[\frac{r_e}{r} \right]^{.57} + C_L \quad 17$$

where the ceiling jet is assumed to be a half Gaussian. Replacing $C_{s0}(r_e)$ using Equations 11 and 13, the maximum smoke concentration at a radial location from plume center in the ceiling jet for $r > 0.18H$ is given by

$$C_{s0}(r) = \frac{\sqrt{2} \left(\frac{\lambda^2}{\lambda^2 + 1} \right) D \dot{Q}_2^{*2/3} \left(\frac{Z_2}{H_2} \right)^{5/3} \left(\frac{r_e}{r} \right)^{.57}}{\left(1 + k \dot{Q}_2^{*2/3} \left(\frac{Z_2}{H_2} \right)^{2/3} \right)} + C_L \quad 18$$

If the smoke yield fraction in equation 8 is replaced with a different yield fraction such as one for carbon monoxide, equation 18 can be used to predict the concentration of that combustion product in the ceiling jet.

Experiment

Experiments were conducted to test the capability of the algorithm to predict CO and smoke concentration in the ceiling jet⁷. The experiments were conducted in a room with floor dimensions of 3.15 m x 3.02 m. A sand burner was centered in the room with the height between the top of the burner and the ceiling being either 2.19 m, 1.50 m or 0.77 m. Two burner geometries were used. The first burner was round with a diameter of 0.085 m while the second burner was square with an effective diameter of 0.194 m. The ceiling was flat and smooth being made up of acoustic ceiling tile. The walls of the room were constructed of glazed cinderblocks.

Instrumentation included thermocouples, CO sensors, a laser to measure obscuration and a tapered element oscillating microbalance (TEOM) to measure smoke concentration. Temperature measurements in the ceiling jet were conducted using bare bead 0.76 mm thermocouples positioned 1 cm below the ceiling at radial positions shown in figure 1. A thermocouple tree located 60 cm from plume center with thermocouples located vertically below the ceiling at (1.0, 3.0, 6.0, 12.0, 24.0, 36.0, 50.0, 75.0 and 100.0) cm were used to measure the depth of the ceiling jet and the temperature in the smoke layer. An aspirated thermocouple was used to check the impact of radiation on the bare bead thermocouples.

The CO measurements were done using electrochemical cells removed from residential CO sensors that were calibrated in the Fire Emulator-Detector Evaluator (FE/DE)⁸ using known CO sources. The FE/DE is designed to produce a controlled velocity and temperature environment where trace impurities from either gas containers or small fires can be added to test commercial sensors. Figure 1 provides the layout for the CO sensors with a CO sensor tree consisting of a sensor at the ceiling and two additional sensors mounted at 1/3 and 2/3 of the distance between the burner and the ceiling located at 60 cm from fire center. Two sensors were located along the same radius and were used to check the radial dependence of the theory with measurement.

Smoke obscuration measurements were conducted using a helium-neon laser mounted such that the laser beam was located 1.0 m from the plume centerline, 6.4 cm beneath the ceiling and had a path length of 0.5 m as shown in figure 2. By measuring the decrease in intensity of the beam, the smoke density is deduced from the light extinction coefficient using the extinction coefficient per unit mass⁹, $8.71 \text{ m}^2/\text{kg}$.

A TEOM was used as a second method of measuring smoke concentration. The sampling tube for the TEOM was positioned 4.4 cm beneath the ceiling and 1.0 m from the plume centerline.

Two fuels, propane (C_3H_8) and propene (C_3H_6), were used for the experiments. Values for the heat of combustion, radiation fraction, smoke yield and CO yield for these fuels are taken from the literature^{10 11 12 13 14} and tabulated below. The calculations were done using the values of Tewarson⁹. Differences in the yield fractions and heat of combustion enter the calculations linearly. Differences in radiation fraction will have a small and nonlinear impact on the calculations as the depth of the smoke layer will be impacted as well as values in the correlation developed above.

Ref #	Smoke Mass Fraction, Y_s Propane/Propene (g/g)	CO Mass Fraction, Y_{co} Propane/Propene (g/g)	Radiation Fract., χ_r Propane/Propene	Heat of Comb., h_c Propane/Propene kJ/g
9	0.024/0.095	0.005/0.017	0.27/0.32	43.7/40.5
10	0.021/0.074	x	x	x
11	0.010/0.069	x	0.28/0.40	x
12	x/x	x	0.27/0.38	x
13	0.0045/x	x	0.27/x	x

The thermocouple measurements were consistent to within 1 °C while the uncertainty in the CO measurements and smoke measurements are still under investigation. The experiments were reproducible in temperature profile as the fire source was a gas burner with a controlled mass flow rate.

Results

An experiment using the 0.085 m diameter round burner located 2.19 m from the ceiling and burning propene will be compared with the algorithm. The complete set of experiments using both propene and propane are available in reference 7. Figure 2 shows the development of the temperature structure in the room using the thermocouple tree located at 60 cm from fire center. The burner is ignited at 180 s and a ceiling jet is observed which extends down to at least 12 cm beneath the ceiling. Within 25 s, the layer forms and is at an almost uniform temperature between 24 cm and 75 cm from the ceiling. Figure 3 presents a comparison of the predictions of the algorithm with the

measurements from a CO sensor located 60 cm from plume center. The calculation was started at 0 seconds which corresponds to 180 s for the experiment. The values for layer temperature and layer height used in the algorithm were calculated using the zone model JET.¹⁵ The CO in the layer and ceiling jet were calculated using the CO mass fraction of reference 9 assuming a steady fire of 2.5 kW starting at 180 s. The measurements would be expected to lie somewhere between the layer values and the maximum ceiling jet values but lie below the calculated CO volume fraction in the layer. A zone model starts forming a layer at the ceiling at the start of the fire while in reality, it takes some time for the ceiling jet to hit the walls, turn and flow back toward the fire to form the layer.

The algorithm was re-evaluated using the measured CO volume fraction of the layer from a sensor at 73 cm from the ceiling as shown in figure 4. Since a layer does not form for the first 70 s, the 3×10^{-6} calculated CO volume fraction represents the unconfined ceiling jet value. The CO sensor in the ceiling jet at 60 cm measures an increasing CO volume fraction starting 30 s after ignition. This volume fraction approaches the calculated value for the unconfined ceiling jet at which point the layer starts to form and the measured and calculated volume fractions track each other to within 1×10^{-6} for the duration of the experiment.

This comparison was repeated for the propene experiment with the burner located 1.5 m from the ceiling. The 30 s delay time for the start of the ceiling jet and the 40 s linear ramp for the initial ceiling jet that was observed in the 2.19 m experiment were included in the calculation. This calculation is in excellent agreement with the measured CO volume fraction in the ceiling jet as shown in figure 5. To successfully model the CO volume fraction in the ceiling jet, the formation time of the layer and response time of the sensor must be included in the calculation.

Figure 6 presents the comparison between the measured smoke density and the calculated smoke density for the upper layer and the maximum value in the ceiling jet using two different smoke mass fractions. The measured value, deduced from the extinction of the laser light, lies either just below or passes through the predicted values. The slope of the measured values is initially in agreement with the calculation but then becomes substantially larger. The measured values from the TEOM are consistently below both the laser measurement and the predicted values. The TEOM measures the mass density of the smoke while the laser measures the light scattering area of the smoke particles. The change in slope of the laser signal later in the experiment may be due to a heating effect as the laser and diode sensor are located in the fire room near the floor. If the formation time for the smoke density in the layer were included as was done for the CO volume fraction in the layer, the smoke density calculation in the ceiling jet would be closer to the value measured by the TEOM. Including a response time for the TEOM would improve the comparison as the TEOM appears to have a lag time of roughly 30 s in responding to the smoke while the laser responds instantaneously. Using one of the smaller yield factors as shown in figure 6 also improves the comparison between experiment and theory but without the smoke layer measurement it is difficult to justify changing constants.

Sensor-Driven Fire Model

Version 1.2 of the sensor-driven fire model, SDFM, is designed to predict the heat release rate (HRR) of a fire based on signals from either smoke or heat sensors positioned below the ceiling that sample the ceiling jet produced by the fire. The estimated HRR is then used by a variant of the zone model CFAST to predict layer temperature and heights in the fire room and in the adjacent rooms in the building. Based on the predicted layer temperature and height, room conditions such as limited visibility and flashover potential can be deduced. In non-fire situations, the SDFM is designed to look for sensor failure, to discriminate between nuisance signals and fire-induced signals, and to monitor the condition of sensors that degrade over time.

When the model receives a sensor signal that indicates a HRR increasing with time and has reached a target threshold, the model will try to verify that it is a true fire by assessing the signals received by other available sensors in the area. Such sensors might include CO or CO₂ sensors as well as heat or smoke sensors. If other sensors do not support the fire signal, a trouble signal will be issued and the program will revert to its normal sensor polling. If no other sensors are available in the room or if other sensors also support the presence of a fire, a fire alarm will be issued.

The target threshold for the model to start checking for a fire is based on two alternative methods of defining a fire signal. The first method used by the model is to compare the sensor signal with a user prescribed signal. This signal would be one that has been developed by observing the response of the sensor to small test fires. The second method would be based on looking at the time history of the sensor signal once a target HRR based on the sensor signal has been reached. If the sensor signal indicates a time growing hazard that has reached a particular HRR, a fire alarm will be issued. This second method may allow for earlier detection of fires as well as fewer false alarms since it depends on a time history as well as a signal magnitude.

The determination of a HRR from a sensor signal requires knowledge about the characteristics of the sensor and its position with respect to the fire. Sensor characteristics include the calibration curve for the analog/digital signal generated by the sensor as a function of temperature or smoke/gas concentration and the delay time introduced by thermal lag or flow conditions into the sensing element. Once the sensor characteristics have been defined, the HRR may be estimated using modeling correlations coupled with a zone fire model. In the following discussion, it will be assumed that only one sensor is present in each room. The sensor will be located close to the ceiling where it can be considered in the ceiling jet. Presently, version 1.2 of SDFM contains algorithms to estimate HRR from either the excess temperature or the smoke concentration in the ceiling jet.

Estimating the Extent of Fire Hazards

Once a HRR has been obtained for one or more of the identified fire sources, this information will be passed to a variant of CFAST in order to calculate layer height, temperatures and smoke concentrations in each room of the structure. From this information, hazards such as limited sight, high temperatures, toxic gases and potential for flashover may be identified on a room-by-room basis for the current fire conditions. The layer temperatures and smoke concentrations calculated using CFAST are also used to estimate fire spread from the room of origin to adjacent rooms. The signals from sensors in these adjacent rooms are compared with calculated signals based on the estimated layer temperature and smoke concentration predicted by CFAST. If the ceiling jet temperature as estimated from sensor signals is 30 % higher than the upper layer temperature predicted by CFAST, it is assumed that a fire has broken out in the adjacent room. If the predicted upper layer temperature exceeds the flashover temperature, 500 °C, it is assumed that a fire has started in that room. In addition, with a known HRR history, projections can be made using CFAST to estimate fire growth and spread. The present version of SDFM does not have this capability.

Flashover Experiment

The capabilities of the SDFM were tested using a seven room, two story, full-scale fire test (Sharon 2) where the major fuel source was wood pallets and flashover was achieved in the burn room¹⁶. Single thermocouples near the ceiling were used for the SDFM inputs to mimic the response of ceiling mounted heat sensors.

To simulate the Sharon 2 test, the seven room townhouse was divided into eight spaces and thermocouple data was used to provide ceiling jet temperatures in six of the eight spaces. A plan view of the townhouse, showing locations of the instrumentation, is shown in figure 7. In the simulation, room 2 was partitioned into a hallway and a room with the thermocouple tree, TC6, providing the temperatures for the hallway. Thermocouple trees TC1, TC2, and TC3 were used to provide data for the upstairs spaces while TC8 and TC4 were used for the other downstairs spaces. The partitioned room 2 on the first floor and the stairway were modeled spaces with no thermocouple measurements. Only the thermocouple near the ceiling was used for the input data from each tree.

The first 231 s of the fire were modeled for the Sharon 2 fire since, in the experiment the wood pallets in the fire room began to fall off the load cell after this time. Figures 8 and 9 provide a comparison of a representative layer temperature as measured by the thermocouple trees with the layer temperature calculated by the model for each room. Agreement between the calculations and the measurements is quite good for all rooms although the model tends to over predict the temperature. The experimental layer height was determined by estimating the location of the midpoint of the temperature transition between the lower layer temperature and the upper layer temperature. The location of the midpoint above the floor was taken as the upper layer height. The calculated layer heights agree well with the estimated layer heights for most of the comparison interval. Only at

the last time intervals for the second floor bedrooms do the calculated upper layer heights drop significantly below the estimated layer heights.

The SDFM is designed to provide information concerning the fire threat that fire fighters might encounter in a building. The fire threats presently in the model include: a smoke layer less than 2 m above the floor (limited visibility), a smoke layer above a temperature of 50 °C and layer height below 1.5 m (toxic gas/thermal hazard), and a smoke layer at a temperature higher than 500 °C (flashover). A comparison of the SDFM predictions with the experimental measurements is given in the table below. The SDFM was run with a reporting interval of 20 s.

The predicted fire threats correlated well with the estimated occurrence of these threats for the lower level rooms using the data shown in table 2 below. The layer heights were predicted to be lower for the upper level rooms than measured which accounts for most of the differences shown in the table for these rooms. For the bedrooms, the smoke in the room may become well mixed with a two-layer structure beginning to disappear. The cycle time for the calculations and measurements was 12 s, meaning those two or three calculations or measurement times produced several of the time differences.

Room	Burn		LL		UL		N		S	
	EX	SD	EX	SD	EX	SD	EX	SD	EX	SD
Visibility Limited	24	12	49	12	88	24	78	49	80	36
Toxic Gas – Thermal Hazard	24	12	49	24	99	36	103	61	94	49
Flashover	48	24	97	97	nr	nr	nr	nr	nr	nr

Table 1 The table presents a comparison of the times in seconds between the experiment (EX) and the SDFM (SD) for the hazard conditions in the burn room (Burn), the lower level (LL) hall, the upper level (UL) hall and the two upper level bedrooms labeled N (north) and S (south). The symbol “nr” indicates that this condition was not reached.

Summary

The goal for the SDFM is to provide adequate warning of fire threats within a structure using the building sensors. Fire warnings issued by the SDFM for the Sharon 2 test were within 65 s or less of the time when the hazard occurred in all rooms and the warnings were conservative. This agreement was obtained using data from only one sensor per

room. Additional sensors in each room would permit the fire source to be more accurately located and as a result better predictive capabilities would be expected.

The smoke/CO ceiling jet algorithm predicted the volume fraction for CO in the ceiling jet to within 2×10^{-6} of the measured value when the measured layer volume fraction was used in the calculation. To get this accuracy using a zone model, the development of the layer must be consistent with the time required for the ceiling jet to flow across the ceiling and the detector response must be included in the algorithm. Additional measurements need to be performed to test the smoke density prediction of the algorithm. The discrepancy in the two smoke measurements needs to be sorted out and the smoke density in the layer must be measured.

The performance of the ceiling jet algorithm needs to be tested in buildings that contain HVAC systems. There are additional algorithms that need to be added or expanded in the SDFM. These algorithms include but are not limited to improving the multiple sensor algorithm for a single room, adding lag time algorithms for sensors, expanding the false alarm algorithm, and adding a wall heating algorithm in order to predict structural failure.

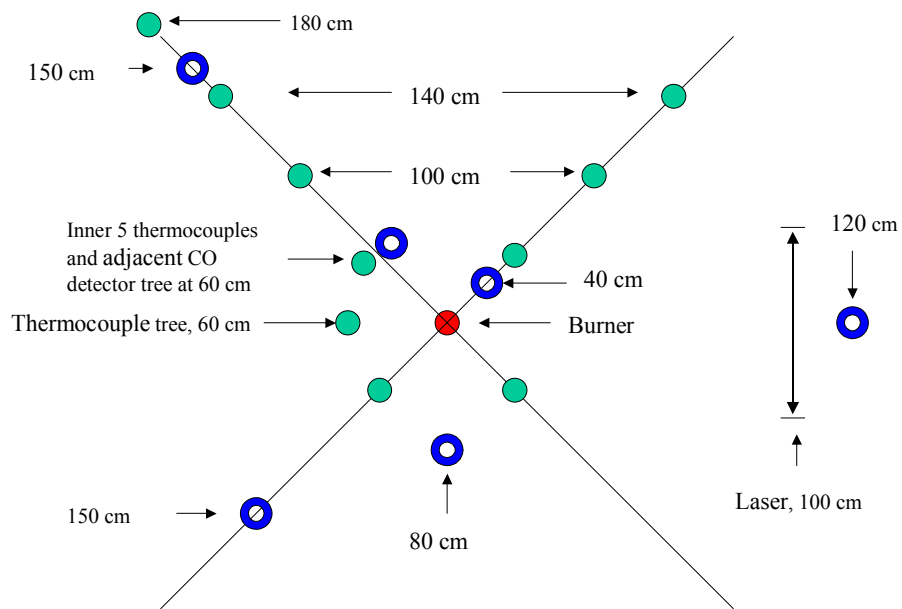


Figure 1 Location of thermocouples (circles), CO sensors (donuts) and laser beam with respect to the burner.

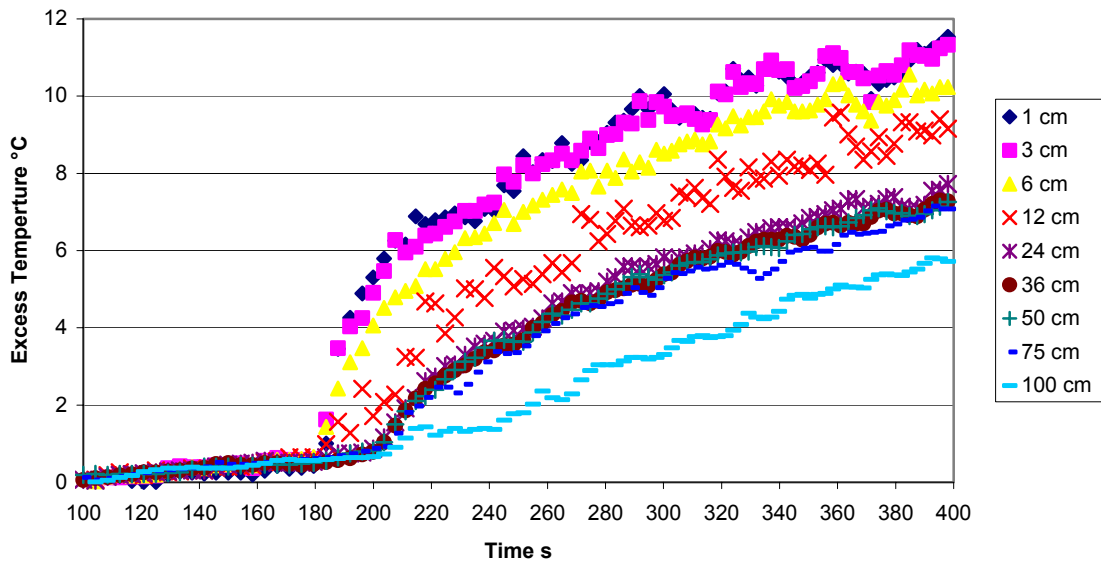


Figure 2 Thermocouple measurements at 60 cm for the 2.19 m propene fire.

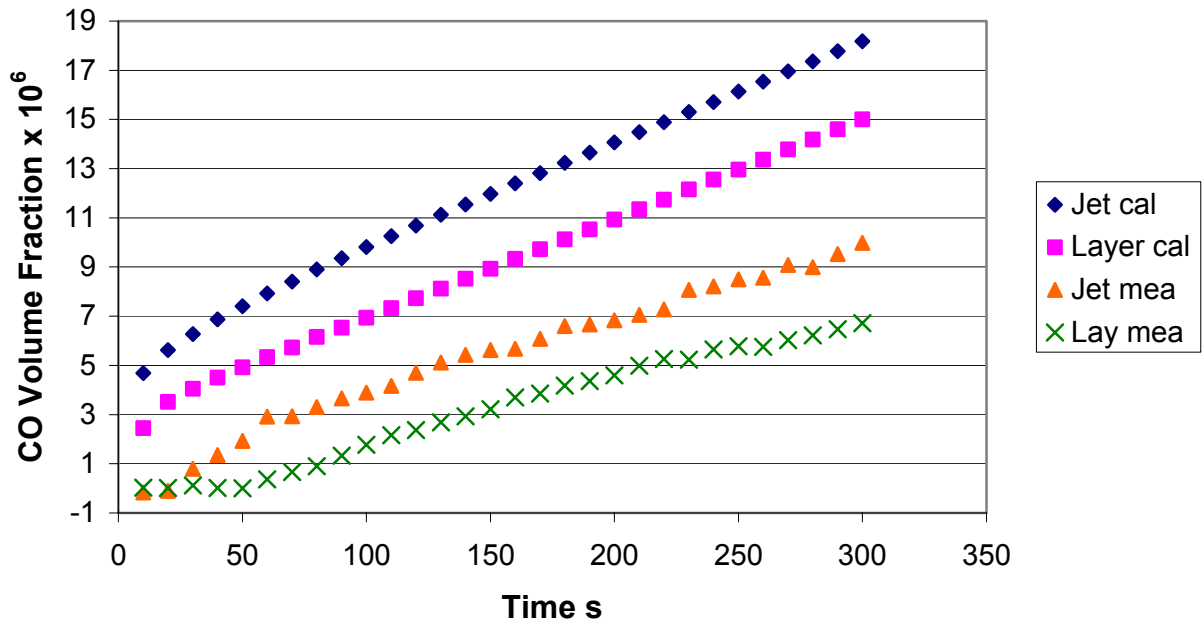


Figure 3 Calculated (cal) and measured (mea) values of CO volume fraction at 60 cm from the fire for the 2.19 m propene experiment.

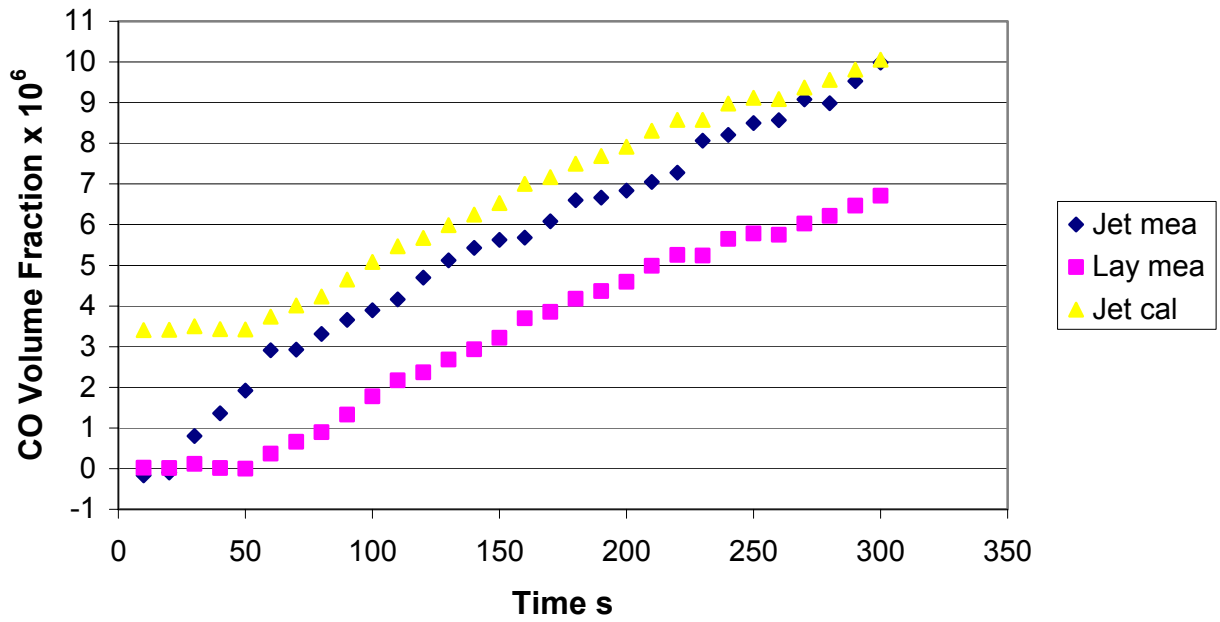


Figure 4 Ceiling jet calculation using the measured CO layer volume fraction for the 2.19 m propene experiment.

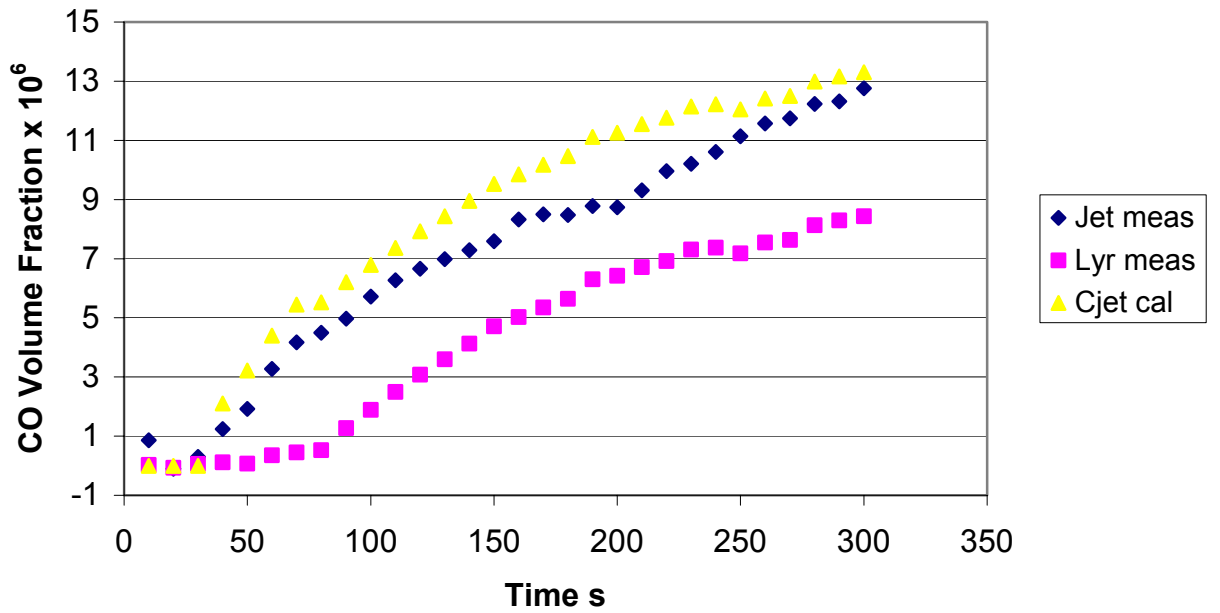


Figure 5 Ceiling jet calculation using the measured CO layer volume fraction for the 1.5 m propene experiment. Included in the calculation is a 30 s delay in starting the ceiling jet and then a linear ramp to maximum fire size of 40 s.

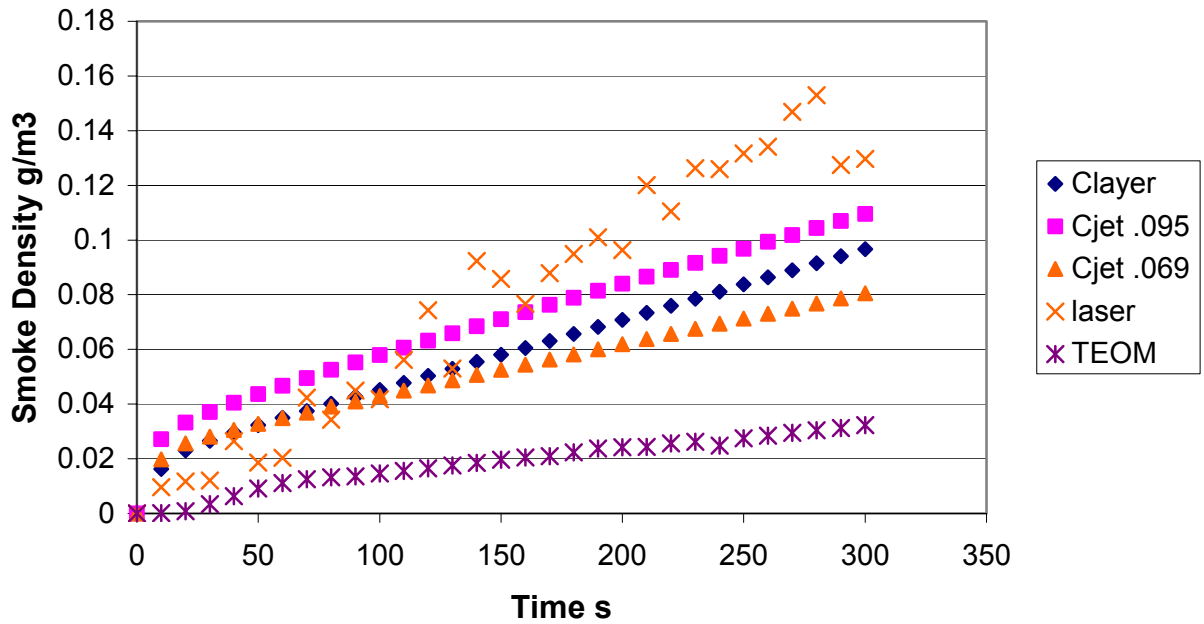


Figure 6 Calculated value of the smoke concentration in the ceiling jet using JET with smoke yield fractions of 0.095 and 0.069 compared with measured values.

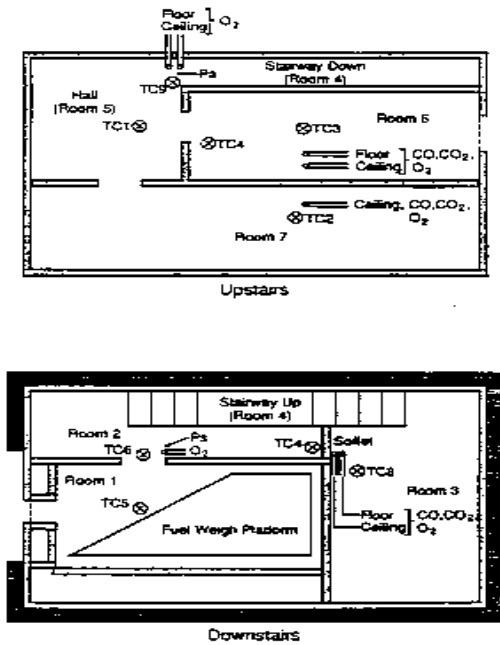


Figure 7 Plan view of Sharon2 townhouse. Thermocouple trees are indicated by TC#.

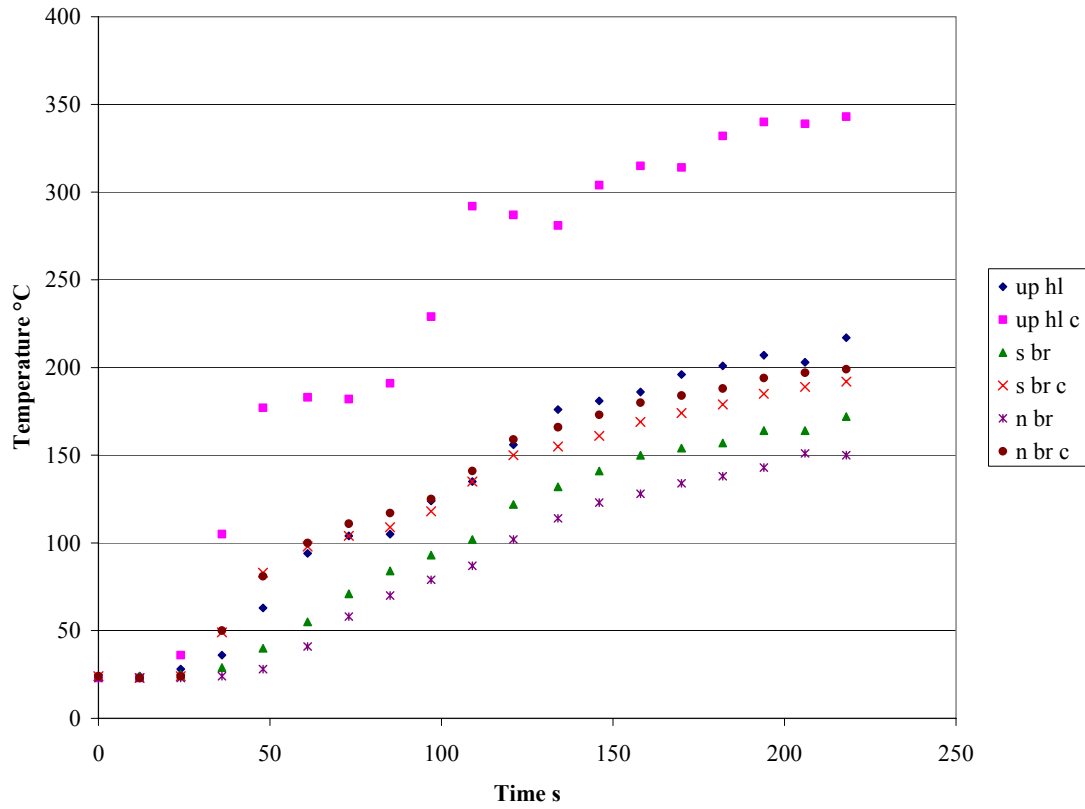


Figure 8 Upstairs hall (up hl) and north and south bedroom (n br and s br) measured and calculated (c) temperature comparisons.

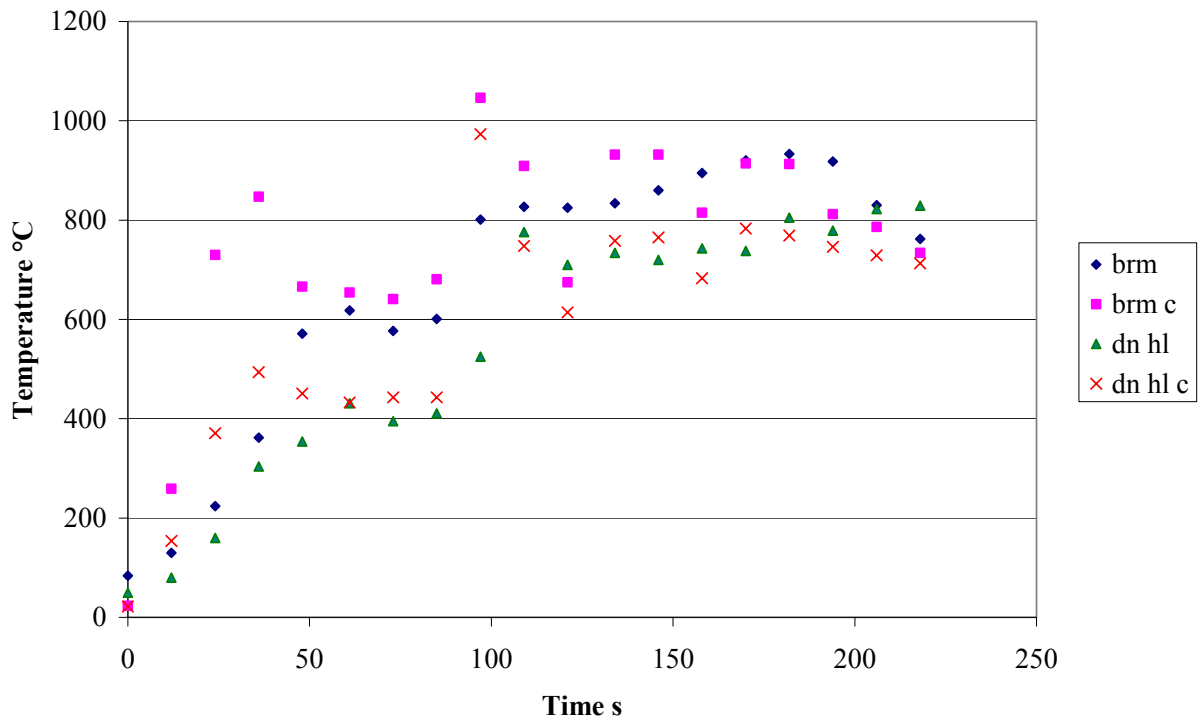


Figure 9 Burn room (brm) and downstairs hall (dn hl) measured and calculated (c) temperature comparisons.

-
- ¹ Nelson, H. E. “Functional Programming/Research Planning for High Technology Federal Office buildings”, *National Institute of Standards and Technology*, NBSIR 84-2828, 1984, pp. 1-28.
- ² Davis, W., D. and Reneke, P. “Predicting Smoke Concentration in the Ceiling Jet”, *National Institute of Standards and Technology*, NISTIR 6480, 2000, pp. 1-12.
- ³ Heskestad, G., “Engineering Relations for Fire Plumes”, *Fire Safety J.*, 7, 1984, pp. 25-32.
- ⁴ Alpert, R. L., “Turbulent Ceiling-Jet Induced by Large-Scale Fires”, *Combustion Science and Technology*, 1975, pp.197-213.
- ⁵ Yamauchi, Yukio, “Prediction of Response Time of Smoke Detectors in Enclosure Fires”, *National Institute of Standards and Technology*, NBSIR88-3707, 1988, pp. 1-46.
- ⁶ Alpert, R., L., “Calculation of Response Time of Ceiling-Mounted Fire Detectors”, *Fire Technology*, 8, 1972, pp. 181-195.
- ⁷ Davis, W. D., Cleary, T., Donnelly, M., and Hellerman, S., “Predicting Smoke and Carbon Monoxide Concentration in the Ceiling Jet in the Presence of a Smoke Layer”, *National Institute of Standards and Technology*”, to be published.
- ⁸ Grosshandler, W. “Toward the Development of a Universal Fire Emulator-Detector Evaluator”, *Fire Safety J.*, 29, 1997, pp. 113 – 128.
- ⁹ Mulholland, G. W. and Croarkin, C., “Specific Extinction Coefficient of Flame Generated Smoke”, *Fire and Materials*, 24, 2000, pp. 227-230.
- ¹⁰ Tewarson, A., “Generation of Heat and Chemical Compounds in Fires”, *The SFPE Handbook of Fire Protection Engineering*, NFPA, 1995, pp. 3-53 - 3-124.
- ¹¹ Newman, J. S., and Steciak, J., “Characterization of Particulates from Diffusion Flames”, *Combustion and Flame*, 67, 1987, pp. 55-64.
- ¹² Kounalakis, M. E., Sivathanu, Y. R., and Faeth, G. M., “Structure and Radiation Properties of Turbulent Nonluminous and Luminous Diffusion Flames”, *NIST Grant 60nanb5d0576*, 1988, pp. 1-78.
- ¹³ Orloff, L., de Ris, J., and Delichatsios, M. A., “Radiation From Buoyant Turbulent Diffusion Flames”, *Factory Mutual Research Corporation*, FMRC J. I. OTOJ7.BU, 1991, pp. 1-16.
- ¹⁴ Becker, H. A. and Liang, D., “Total Emission of Soot and Thermal Radiation by Free Turbulent Diffusion Flames”, *Combustion and Flame*, 44, 1982, pp. 305-318.

-
- ¹⁵ Davis, W. D., “The Zone Fire Model JET: A Model for the Prediction of Detector Activation and Gas Temperature in the Presence of a Smoke Layer”, NISTIR 6324, *National Institute of Standards and Technology*, 1999, pp. 1-51.
- ¹⁶ Levine, R. S. and Nelson, H. E., “Full Scale Simulation of a Fatal Fire and Comparison of Results with Two Multiroom Models Volume II – DATA”, *National Institute of Standards and Technology*, NISTIR 90-4268, 1990, pp. 1-125.